

# Effect of Li Content, Deposition Time and Solution Concentration on Morphology and Photoluminescence Properties of $Y_2O_3: 5\%Eu^{3+}, x\%Li^+$ Thin Film

Li Yongqiang<sup>1,2</sup>, Zhang Lingyun<sup>2,3</sup>, Dai Zhenxiang<sup>1,2</sup>, Zheng Ganhong<sup>1,2</sup>, Zhu Yanan<sup>1,2</sup>,  
Ma Yongqing<sup>1,2</sup>

<sup>1</sup> Anhui University, Hefei 230601, China; <sup>2</sup> Anhui Key Laboratory of Information Materials and Devices, Hefei 230601, China; <sup>3</sup> Hefei University, Hefei 230601, China

**Abstract:**  $Y_2O_3: 5\%Eu^{3+}, x\%Li^+$  phosphor thin film was fabricated via an electro-deposited method. The dependence of the morphology and luminescent properties for  $Y_2O_3: 5\%Eu^{3+}, x\%Li^+$  thin film on Li content, deposition time and solution concentration were studied. The results indicate that the morphology and the emission intensity strongly depend on the Li content, deposition time, and solution concentration. It is found that the Li addition is beneficial to the formation of flower morphology and then enhances the photoluminescence intensity. The optimal Li content is 15% for  $Y_2O_3: 5\%Eu^{3+}, x\%Li^+$ .

**Key words:** phosphor thin film; electro-deposited method; Li-doped

$Y_2O_3$  has been investigated due to its superior properties and widely used in white light emitting diodes, plasma display panels, and cathode ray tubes [1-3]. It is well known that  $Li^+$  ions as the dopants play an important role in increasing the luminescent efficiency of bulk and nano-sized phosphors. Wang<sup>[4]</sup> etc. found that the luminescent intensity could be greatly enhanced by doping  $Li^+$  ions in  $Y_2O_3:Ho^{3+}/Yb^{3+}$  and  $Er^{3+}/Li^+$  co-doped  $Sb_2O_3-Na_2O-SiO_2$  glasses. The phosphors intensity of  $Tm^{3+}$  ions of  $Y_2O_3:Tm^{3+}/Yb^{3+}$  can be enhanced by about 14 times with 5mol%  $Li^+$  ions<sup>[5]</sup>. The reasons for the emission intensity enhancement by doping  $Li^+$  ions are attributed to the modification of the local symmetry around the  $Er^{3+}/Yb^{3+}/Ho^{3+}$  ion, the reduction of OH groups, and the creation of the oxygen vacancies in the phosphors.

Now, various techniques have been developed for  $Y_2O_3:Eu^{3+}$  nano-size compound synthesis over the past decades, typically including combustion<sup>[6]</sup>, sol-gel<sup>[7]</sup>, and thermal plasma processing<sup>[8]</sup>. The phosphor films have also

been prepared using electron-beam evaporation<sup>[9]</sup>, pulsed laser deposition (PLD)<sup>[10]</sup>, sol-gel techniques<sup>[11]</sup>, and electro-deposition<sup>[12]</sup>.

Here, the electro-deposition method was adopted to prepare  $Y_2O_3: 5\%Eu^{3+}, x\%Li^+$  thin film and then morphology and luminescent properties were also probed.

## 1 Experiment

All samples were prepared by electro-deposition in a conventional three-electrode cell. The working electrode was FTO (fluorine doped tin oxide film) coated glass, counter electrode was a platinum foil, and the reference electrode was Ag/AgCl/saturated KCl. The initial materials were  $Y(NO_3)_3 \cdot 6H_2O$ ,  $Eu(NO_3)_3 \cdot 6H_2O$ , and  $LiNO_3$ . Firstly, different amounts of the starting materials  $Y(NO_3)_3 \cdot 6H_2O$ ,  $Eu(NO_3)_3 \cdot 6H_2O$  and  $LiNO_3$  were dissolved in deionized water under stirring and heating until the uniform and transparent solution were formed. The molar concentration of the solution was 0.1 mol/L. Secondly, the

Received date: May 18, 2016

Foundation item: National Natural Science Foundation of China (11204001, 11174004); Anhui Provincial Natural Science Foundation (1308085MA04); Higher Educational Natural Science Foundation of Anhui Province (KJ2013A031); Anhui University Scientific Research Fund (201410357005, KYXL2013009)

Corresponding author: Dai Zhenxiang, Ph. D., Professor, School of Physics and Materials Science, Anhui University, Hefei 230601, P. R. China, Tel: 0086-551-63861258, E-mail: physdai@ahu.edu.cn

Copyright © 2017, Northwest Institute for Nonferrous Metal Research. Published by Elsevier BV. All rights reserved.

above solution was ready for electro-deposition. The applied potential was  $-1.2$  V versus Ag/AgCl/saturated KCl for each sample. The deposition temperature was  $60$  °C for each sample. The deposition time was 0.5, 1.0, and 1.5 h, separately. After deposition, the samples were annealed in air at  $600$  °C. The crystal structures of these samples were characterized by X-ray diffraction using an X-ray diffractometer (XRD, DX-2000 SSC) with Cu K $\alpha$  radiation ( $\lambda=0.15418$  nm) over a scanning range of  $10^\circ \sim 70^\circ$  with a step of  $0.02^\circ$ . Scanning electron microscopy (SEM, S-4800, Hitachi) and high resolution transmission electron microscopy (TEM, JEOL JEM-2100) were used to observe the morphologies and microstructures. FTIR spectra of the phosphor powders were recorded on a Nicolet IR-200 spectrometer with KBr pellet technique from 4000 to  $400$   $\text{cm}^{-1}$ . The excitation and emission spectra were measured on a FL fluorescence spectrophotometer (F-4500, Hitachi). The luminescence lifetime was collected by one EasyLife fluorescence spectrometer. All the measurements were carried out at room temperature.

## 2 Results and Discussion

### 2.1 Effect of Li content on the structure morphology and luminescent properties of $\text{Y}_2\text{O}_3:5\% \text{Eu}^{3+}, x\% \text{Li}^+$

Fig.1 shows XRD patterns of the  $\text{Y}_2\text{O}_3:5\% \text{Eu}^{3+}$  (L00),  $\text{Y}_2\text{O}_3:5\% \text{Eu}^{3+}, 12\% \text{Li}^+$  (L12), and  $\text{Y}_2\text{O}_3:5\% \text{Eu}^{3+}, 21\% \text{Li}^+$  (L21). The XRD patterns are matched with JCPDS (No.89-5592) patterns of  $\text{Y}_2\text{O}_3$ , which has a cubic structure with space group  $\text{Ia}(206)$ . The XRD patterns exhibit standard peaks at  $2\theta$  of  $20.50^\circ$ ;  $29.08^\circ$ ;  $33.74^\circ$ ;  $48.40^\circ$ ; and  $57.50^\circ$  assigned to (211), (222), (400), (440), and (622) planes, respectively. The results show the  $\text{Y}_2\text{O}_3$  lattice is not disturbed by the insertion of  $\text{Eu}^{3+}$  and  $\text{Li}^+$  ions.

The thickness and structure of the films are presented in Fig.2. The thickness is about  $30 \sim 50$   $\mu\text{m}$ . Fig.2c is the low magnification SEM image for  $\text{Y}_2\text{O}_3:5\% \text{Eu}^{3+}, 12\% \text{Li}^+$ . It can be observed that the sample is composed of a large number of uniform flower-like nano-structures, whose average diameter is about  $4$   $\mu\text{m}$ . The close inspection of the high-magnification image reveals that these flowers are made up of many thin petals with a smooth and large surface, and that the thickness is about  $0.5 \sim 1.0$   $\mu\text{m}$  (shown as Fig.2d). Fig.2e shows that the TEM image for  $\text{Y}_2\text{O}_3:5\% \text{Eu}^{3+}, 12\% \text{Li}^+$  has conspicuous hierarchical structures like flowers, which is consistent with the SEM images. A single petal peeled from  $\text{Y}_2\text{O}_3:5\% \text{Eu}^{3+}, 12\% \text{Li}^+$  micro-flower was investigated carefully as shown in Fig.2f. It is clearly found that the petal is composed of a plenty of nano-particles with diameter about  $50$  nm even smaller via the weak self-assembly. In other words, the petals used to construct  $\text{Y}_2\text{O}_3:\text{Eu}^{3+}(5\%), \text{Li}^+(x\%)$  micro-flowers is the

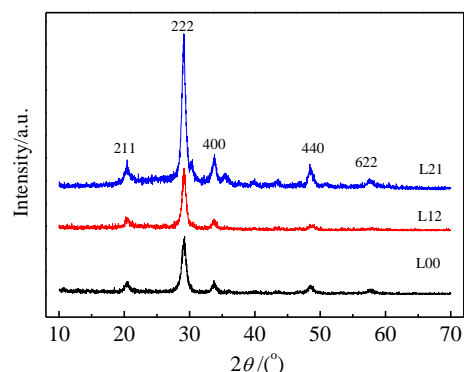


Fig.1 XRD patterns of  $\text{Y}_2\text{O}_3:5\% \text{Eu}^{3+}$  (L00),  $\text{Y}_2\text{O}_3:5\% \text{Eu}^{3+}, 12\% \text{Li}^+$  (L12), and  $\text{Y}_2\text{O}_3:5\% \text{Eu}^{3+}, 21\% \text{Li}^+$  (L21)

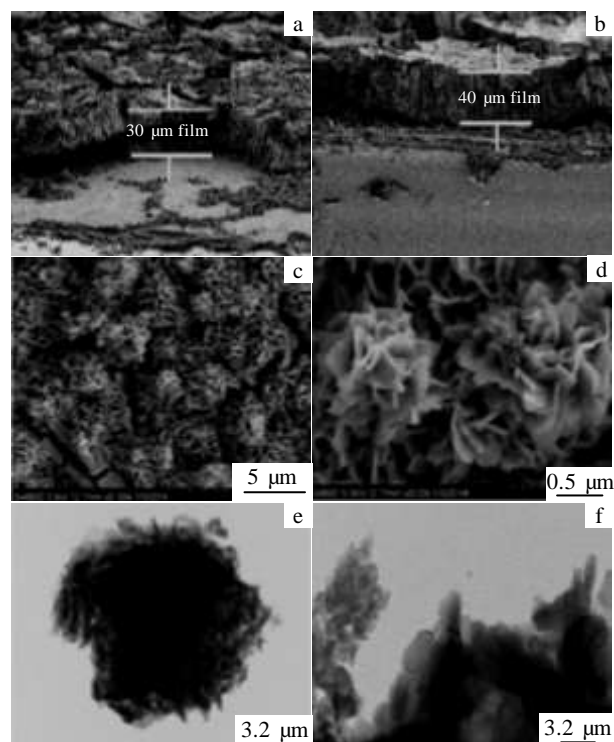


Fig.2 TEM images of cross-section for  $\text{Y}_2\text{O}_3:5\% \text{Eu}^{3+}, 12\% \text{Li}^+$  (a, b); SEM images for  $\text{Y}_2\text{O}_3:5\% \text{Eu}^{3+}, 12\% \text{Li}^+$  with low amplification (c) and with high amplification (d); TEM images for a whole flower (e) and for one petal (f)

collections of nano-particles weakly bond together (as shown in Fig.2f).

To investigate the growth process of the self-assembled flower-like micro-architectures, six different solutions:  $\text{Y}_2\text{O}_3:5\% \text{Eu}^{3+}$ ;  $\text{Y}_2\text{O}_3:5\% \text{Eu}^{3+}, 3\% \text{Li}^+$ ;  $\text{Y}_2\text{O}_3:5\% \text{Eu}^{3+}, 6\% \text{Li}^+$ ;  $\text{Y}_2\text{O}_3:5\% \text{Eu}^{3+}, 12\% \text{Li}^+$ ;  $\text{Y}_2\text{O}_3:5\% \text{Eu}^{3+}, 21\% \text{Li}^+$ ;  $\text{Y}_2\text{O}_3:5\% \text{Eu}^{3+}, 24\% \text{Li}^+$  were prepared with other synthetic conditions remaining unchanged. The morphologies are observed and

shown in Fig.3. Without Li doping, there are many flakes attached with each other and no-flower shapes are observed, as presented in Fig.3a. While with adding 3%Li dopants into the sample, it is clearly seen that these flakes begin to aggregate and the flower-like micro-architectures can be found. As illustrated in Fig.3, these flakes are made of nano-particles, which may be considered as the  $Y_2O_3$  crystal nucleus. This is also popularly explained as the first stage of the formation of other crystal nuclei<sup>[13]</sup>. Tiny nano-particles are assembled automatically to be “flakes” and then assembled again to form initial flower-like structures. For  $Y_2O_3:5\%Eu^{3+}, 24\%Li^+$  sample as shown in Fig.3f, most of the nano-flakes are aggregated each other and no discrete single nano-flakes can be found. With increasing Li concentration, more and more flowers appear, and the flowers also become bigger and bigger as presented in Fig.3.

The excitation spectra (Fig.4a) monitored at 613 nm exhibit sharp excitation lines of the  $Eu^{3+}$  ions, in the longer wavelength region (at 398, 468, and 538 nm). It is attributed to the direct absorption of the  $Eu^{3+}$  ion assigned to transitions of  ${}^7F_0 \rightarrow {}^5L_6$ ,  ${}^7F_0 \rightarrow {}^5D_2$ , and  ${}^7F_1 \rightarrow {}^5D_1$ , respectively. The emission spectra of  $Y_2O_3:Eu^{3+}(5\%), Li^+(x\%)(0 \leq x \leq 24)$  film are given in Fig.4b. The spectra are composed of the well-known lines locating at 598 nm ( ${}^5D_0 \rightarrow {}^7F_4$ ), 618 nm ( ${}^5D_0 \rightarrow {}^7F_2$ ), and 650 nm ( ${}^5D_0 \rightarrow {}^7F_3$ ) upon excitation with 398 nm irradiation. Similar phenomenon has been reported in other  $Eu^{3+}$ -activated red-emitting phosphors<sup>[14]</sup>. The emission intensity are enhanced with the increasing of  $Li^+$  doped content and reaches the highest intensity at  $x=15$ , and then gradually decreases with further increase of Li concentra-

tion. That is to say, the optimal  $Li^+$  doped content in  $Y_2O_3:Eu^{3+}(5\%), Li^+(x\%)(0 \leq x \leq 24)$  phosphor is  $x=15$ .

Fig.5 shows the FT-IR spectra of  $x=0, 6, 12, 15, 18,$  and  $21$  samples. The peaks in the range  $1380 \sim 1500\text{ cm}^{-1}$  and around  $3500\text{ cm}^{-1}$  are assigned to the bending modes and the stretching modes of  $OH^-$  groups, respectively<sup>[15]</sup>. As can be seen from these spectra, the intensity of all impurity peaks becomes weaker when adding  $Li^+$  ions into  $Y_2O_3:Eu^{3+}(5\%), Li^+(x\%)(0 \leq x \leq 24)$  compounds. It indicates that the enhanced photoluminescence intensity may also result from the reducing number of  $OH^-$  groups. Since the  $OH^-$  groups with high vibration frequency can increase the non-radiative relaxation rate and hence decrease photoluminescence efficiency<sup>[4]</sup>. The reduced  $OH^-$  group absorption, as discussed in Fig.5, means the reduction of the  $OH^-$  groups decreases the non-radiative transition probability with  $Li^+$  doping. On the other hand, the incorporation of  $Li^+$  ions creates the oxygen vacancies, which might act as one sensitizer for the effective energy transfer due to the strong mixing of charge transfer states<sup>[16]</sup>. The oxygen vacancies in the surface of the nano-crystals will decrease the luminescence quenching centers and increase the crystallinity, thereby enhancing the emission intensity. With the gradual increase in  $Li^+$  content, the oxygen vacancies of the host lattice greatly increase, which will destroy the emission intensity. So the intensity of photoluminescence will be reinforced as the  $Li^+$  concentration increases from 0% to 15%, and then decline as the  $Li^+$  concentration increases further.

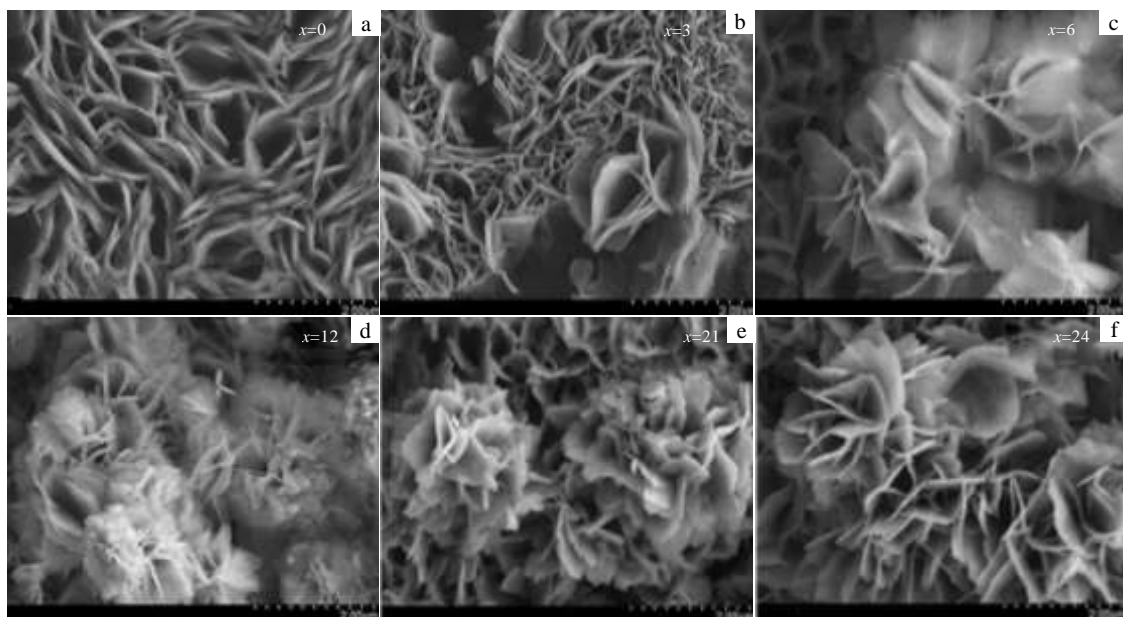


Fig.3 SEM images for  $Y_2O_3:5\%Eu^{3+}$  (a),  $Y_2O_3:5\%Eu^{3+}, 3\%Li^+$  (b),  $Y_2O_3:5\%Eu^{3+}, 6\%Li^+$  (c),  $Y_2O_3:5\%Eu^{3+}, 12\%Li^+$  (d),  $Y_2O_3:5\%Eu^{3+}, 21\%Li^+$  (e), and  $Y_2O_3:5\%Eu^{3+}, 24\%Li^+$  (f)

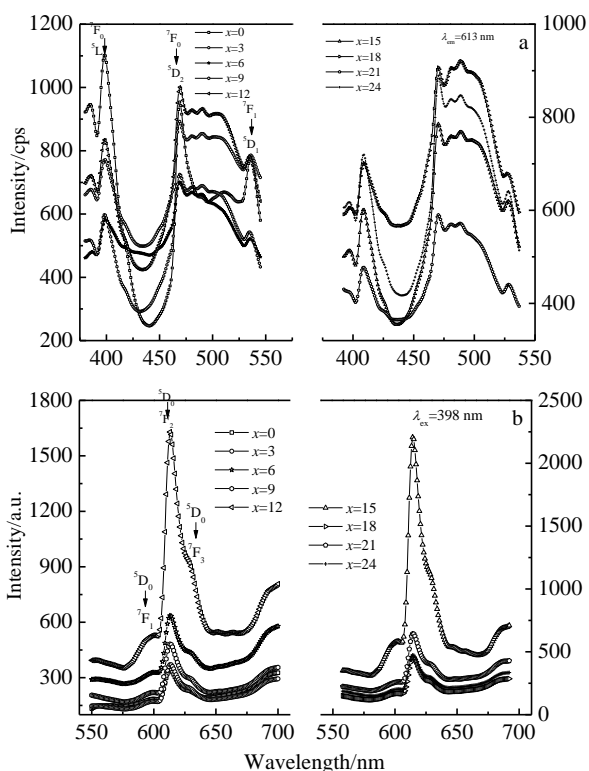


Fig.4 Excitation spectra ( $\lambda_{em}=613$  nm) (a) and emission spectra ( $\lambda_{ex}=398$  nm) (b) for  $Y_2O_3:5\%Eu^{3+}, x\%Li^+$  ( $0 \leq x \leq 24$ ) film

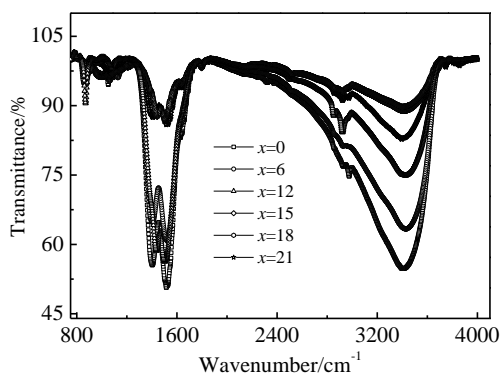


Fig.5 FT-IR spectra for  $Y_2O_3:5\%Eu^{3+}, x\%Li^+$  ( $x=0, 6, 12, 15, 18,$  and  $21$ ) samples

In Fig.6, it is shown that the decay behaviors of the  $^5D_0 \rightarrow ^7F_2$  transition of  $Eu^{3+}$  ( $\lambda_{em}=613$  nm) for  $Y_2O_3:5\%Eu^{3+}, x\%Li^+$  ( $x=0, 12,$  and  $24$ ) samples are excited at 398 nm. All these experimental curves can be well fitted as single exponential functions. The lifetime values are also shown in Fig.6.

## 2.2 Effect of deposition reaction time on the morphology and luminescent properties of $Y_2O_3:5\%Eu^{3+}, 21\%Li^+$

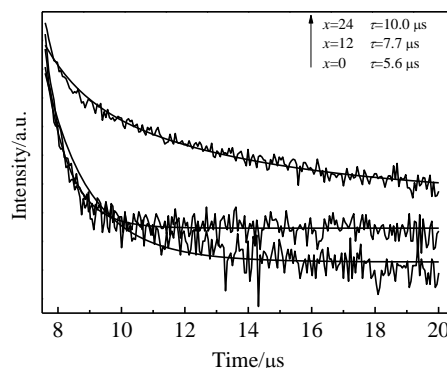
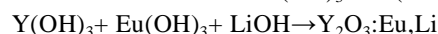
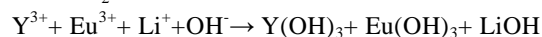
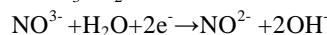
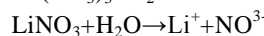
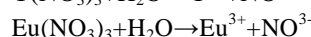
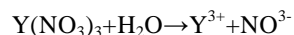


Fig.6 Decay lifetime spectra for the  $^5D_0 \rightarrow ^7F_2$  transition of  $Y_2O_3:5\%Eu^{3+}, x\%Li^+$  ( $x=0, 12,$  and  $21$ ) samples

To investigate the growth mechanism of such flower-like nano-structures further, we take the  $Y_2O_3:5\%Eu^{3+}, 21\%Li^+$  as an example to investigate the effect of different electro-deposition time on the micro-morphology and luminescent properties.

In the current study, cell reactions occurring with the applied electric field are as follows:



After the electric potential was applied on the cell, the free  $Y^{3+}$ ,  $Eu^{3+}$ , and  $Li^+$  ions in the solution would be moved toward the cathode (ITO substrate) and condensed to Y, Eu, and Li droplets. These Y, Eu, and Li droplets reacted with hydroxide to form  $Y(OH)_3$ ,  $Eu(OH)_3$  and  $LiOH$ . The amount of  $Y^{3+}$ ,  $Eu^{3+}$ , and  $Li^+$  ions, which are condensed on the ITO glass, increased with delaying the deposition time. As a result, the diameter and shape of the nano-flower core would be increased, as shown in Fig.7. Fig.7a, 7b, and 7c present the SEM morphologies for the deposition time of 0.5, 1.0, and 1.5 h, respectively. The product is totally composed of flower-like nano-structure. After the deposition for 0.5 h as shown in Fig.7a, the products exhibit the flower-like morphology. However, comparing with the samples obtained after depositing for 1.0 h and 1.5 h, these flowers are less and irregular. As the deposition time has proceeded for 1 h, the sample exhibits totally flower-like morphology, except that only some smaller flowers exist as shown in Fig.7b. Fig.7c is the sample for the deposition time of 1.5 h, and the sample is totally composed of the uniform nano-flowers. Based on the time-dependent experiment, a so-called three step process was proposed for the formation of the flower-like nano-structure<sup>[17]</sup>.

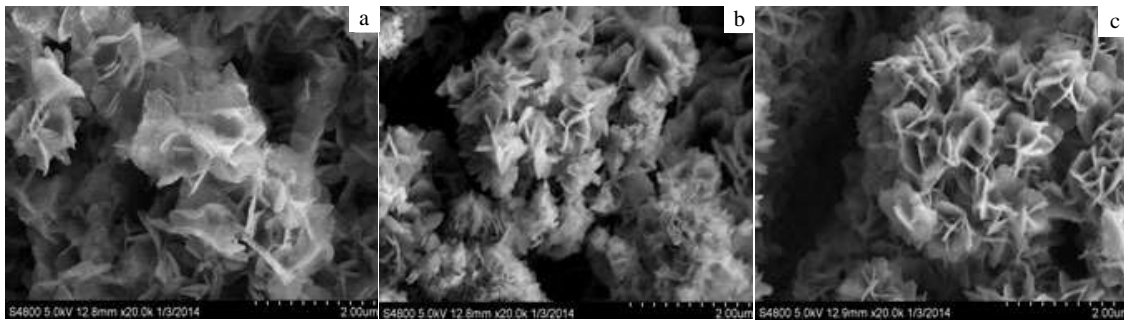


Fig.7 SEM morphologies of  $Y_2O_3:5\%Eu^{3+}, 21\%Li^+$  for different deposition time: (a) 0.5 h, (b) 1.0 h, and (c) 1.5 h

The emission spectra of  $Y_2O_3:5\%Eu^{3+}, 21\%Li^+$  with different deposition time were also studied. The obtained results are presented in Fig.8. Obviously, the emission intensity is enhanced with the increasing of deposition time. This suggests that more  $Eu^{3+}$  ions are deposited in  $Y_2O_3:Eu^{3+}(5\%), Li^+(21\%)$  thin film. The variation of emission intensity with the deposition time may be related to the micro-structure during the growth process as shown in Fig.7. The highest emission intensity grown for 1.5 h deposition has the largest and the most regular nano-flower.

**2.3 Effect of concentration of the solution on the morphology and luminescent properties of  $Y_2O_3:5\%Eu^{3+}, 24\%Li^+$**

Fig.9a and 9b present the SEM images of the obtained samples  $Y_2O_3:5\%Eu^{3+}, 24\%Li^+$  when the concentration of solution is 0.08 and 0.10 mol/L, respectively. In the solution, higher solution concentration means more particles, resulting in the adequate growth of the nano-flakes and the aggregation of the flowers. The emission intensities of 0.08 and 0.10 mol/L of  $Y_2O_3:5\%Eu^{3+}, 24\%Li^+$  film are shown in Fig.10. Obviously, in the case of higher concentration solution with more particles, the stronger emission intensity is observed.

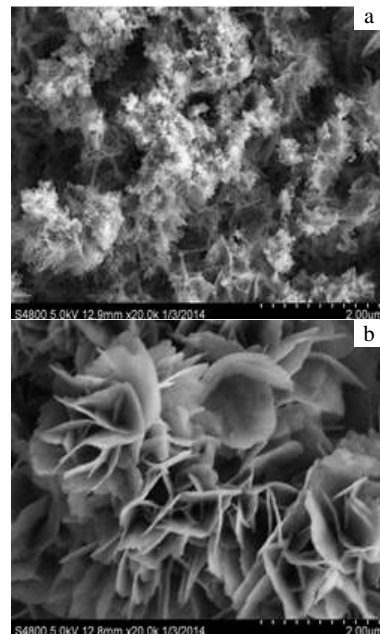


Fig.9 SEM images of  $Y_2O_3:5\%Eu^{3+}, 24\%Li^+$  film for different concentrations of solution: (a) 0.08 mol/L and (b) 0.10 mol/L

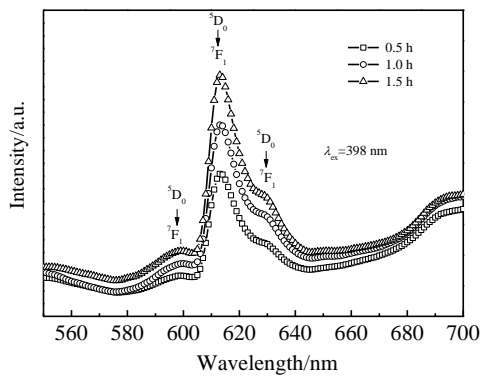


Fig.8 Emission spectra of  $Y_2O_3:5\%Eu^{3+}, 21\%Li^+$  for different deposition time

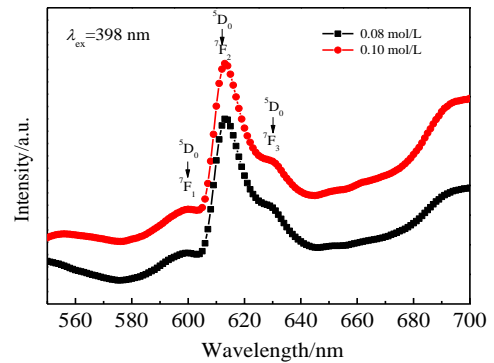


Fig.10 Emission intensity of  $Y_2O_3:5\%Eu^{3+}, 24\%Li^+$  film for different concentrations of solution

### 3 Conclusions

1)  $\text{Y}_2\text{O}_3: 5\% \text{Eu}^{3+}, x\% \text{Li}^+$  phosphor thin film can be prepared by electro-deposited method. Doped  $\text{Li}^+$  ions do not change the structure of  $\text{Y}_2\text{O}_3:\text{Eu}^{3+}$ . The samples are composed of a large number of uniform nano-structure flakes. With Li doping, the flakes aggregate gradually and the flower-like micro-architectures are observed.

2) The emission intensity is enhanced with Li doping level increasing from 0 to 15%, and then declines with Li doping further.

3) The deposition time and solution concentration are also important factors determining the morphology and the emission intensity of  $\text{Y}_2\text{O}_3: 5\% \text{Eu}^{3+}, x\% \text{Li}^+$  thin film.

### References

- 1 Wang J Q, Yang S, Cao Z J et al. *Rare Metal Materials and Engineering*[J], 2014, 43(10): 2316
- 2 Zhang J H, Hao Z D, Li J et al. *Light: Science & Applications*[J], 2015, 4: 239
- 3 Miao H, Ji R N, Hu X Y et al. *Journal of Alloys and Compounds*[J], 2015, 629: 74
- 4 Bai X F, Wang Y X, Peng G Y et al. *Journal of Alloys and Compound*[J], 2009, 478: 676
- 5 Liu L, Wang Y, Bai Y et al. *Journal of Applied Physics* [J], 2010, 107: 93103
- 6 Ekambaram S, Patil K C. *Journal of Alloys and Compound*[J], 2005, 393: 81
- 7 Lin J, Yu M, Lin C L et al. *Journal of Physics Chemical C*[J], 2007, 111: 5835
- 8 Camenzind A, Strobel R, Krumeich F et al. *Advanced Powder Technology*[J], 2007, 18: 5
- 9 Sharma R N, Lakshami S T, Rastogi A C. *Thin Solid Films* [J], 1991, 199: 1
- 10 Cho K G, Kumar D, Lee D G et al. *Applied Physics Letter*[J], 1997, 71: 3335
- 11 Rao R. *Solid State Communication*[J], 1996, 99: 439
- 12 Wang L, Liao N, Zeng H et al. *Thin Solid Films*[J], 2011, 520: 174
- 13 Jana T K, Pal A, Chatterjee K. *Journal of Alloys and Compounds*[J], 2014, 584: 510
- 14 Ju G F, Hun Y H, Chen L et al. *Journal of Luminescence*[J], 2012, 132: 1853
- 15 Mishra K, Giri N, Rai S. *Applied of Physics B*[J], 2011, 103: 863
- 16 Yi S, Bae J S, Moon B K et al. *Applied Physics Letter*[J], 2002, 81: 3344
- 17 Park J, Privman V, Matijevic E. *Journal of Physics Chemical B*[J], 2001, 105: 11 630

## Li 含量、沉淀时间以及溶液浓度对 $\text{Y}_2\text{O}_3: 5\% \text{Eu}^{3+}, x\% \text{Li}^+$ 薄膜的形貌和光学性能的影响

李勇强<sup>1,2</sup>, 张凌云<sup>2,3</sup>, 戴振翔<sup>1,2</sup>, 郑赣鸿<sup>1,2</sup>, 朱亚男<sup>1,2</sup>, 马永青<sup>1,2</sup>

(1. 安徽大学, 安徽 合肥 230601)

(2. 安徽省信息材料与器件重点实验室, 安徽 合肥 230601)

(3. 合肥学院, 安徽 合肥 230601)

**摘要:** 利用电化学沉积法制备 Li 掺杂的  $\text{Y}_2\text{O}_3: 5\% \text{Eu}^{3+}, x\% \text{Li}^+$  荧光薄膜, 并且研究了 Li 含量, 沉积时间和溶液浓度对样品的表面形貌和发光强度的影响。结果表明, 上述三者对所制备的  $\text{Y}_2\text{O}_3: 5\% \text{Eu}^{3+}, x\% \text{Li}^+$  荧光发光薄膜的形貌和发光性能均有影响。并且当  $x=15$  时, 样品的形貌和发光强度表现最佳。

**关键词:** 荧光发光薄膜; 电化学沉积; Li 离子掺杂

**作者简介:** 李勇强, 男, 1989 年生, 硕士生, 安徽大学物理与材料科学学院, 安徽 合肥 230601, 电话: 0551-63861258, E-mail: 745076060@qq.com